IJE | INDONESIAN JOURNAL OF ENERGY
P-ISSN: 2549-1016 | E-ISSN: 2549-760X
available online at www.ije-pyc.org
Published by: The Purnomo Yusgiantoro Center

Finite Element Analysis of Structural Integrity and Fatigue Life of Char Removal System in High-Temperature Gasification

Nina K. Supriatna [1,*], Agung T. Kuncoro [2], Bayu A. Saputro [3], Muhammad Iksanudin [4], Silviana Simbolon [2], Muhammad Yunus [5], Prima Zuldian [1], Agus Kismanto [6], Maulana Arifin [1], Raden I. Purawiardi [1]

[1] Research Center for Energy Conversion Technology, Badan Riset dan Inovasi Nasional, KST BJ Habibie, Serpong, Tangerang Selatan 15314, Indonesia
[2] Department of Mechanical Engineering, Universitas Pamulang, Jl. Rajawali G No.33, Pamulang Barat, Tangerang Selatan 15417, Indonesia
[3] Department of Automotive and Mechanical Engineering, Universitas Muhammadiyah Magelang, Jl. Mayjen Bambang Soegeng, Glagak, Sumberrejo, Kabupaten Magelang 56172, Indonesia
[4] Department of Mechanical Engineering, Universitas Gajah Mada, Bulaksumur, Caturtunggal, Kabupaten Sleman 55281, Indonesia
[5] Research Center for Nuclear Reactor Technology, Badan Riset dan Inovasi Nasional, KST BJ Habibie, Serpong, Tangerang Selatan 15314, Indonesia
[6] Research Center for Fuel Technology, Badan Riset dan Inovasi Nasional, KST BJ Habibie, Serpong, Tangerang Selatan 15314, Indonesia

*Corresponding Author: nina016@brin.go.id

Article History

Received 2 May 2026
Accepted 9 June 2026
Available 31 August 2026

Abstract

Biomass gasification is a crucial technology for sustainable energy conversion; however, its continuous operation and overall efficiency are heavily dependent on the reliable extraction of solid by-products. This study investigates the structural integrity and fatigue life of a char removal system used in high-temperature biomass gasification. The system operates under severe thermo-mechanical conditions, including elevated temperatures and varying mechanical loads, which may lead to structural degradation and failure. A Finite Element Analysis (FEA) approach using ANSYS was employed to evaluate the performance of ASTM A36 steel under mechanical loads of 100 kg, 150 kg, and 200 kg, combined with thermal conditions of 800 °C, 1,000 °C, and 1,200 °C. Key parameters analyzed include equivalent stress, elastic strain, total deformation, safety factor, and fatigue life. The results indicate that while temperature variations have minimal influence on peak stress values, they significantly affect the distribution of strain and deformation due to material stiffness degradation. In contrast, mechanical loading has a dominant impact on structural performance, leading to increased stress, deformation, and reduced safety factors. Fatigue analysis reveals that while the structure maintains a theoretical infinite design life of 1×10^6 cycles across all loads, the minimum fatigue safety factor drops significantly from 2.92 at 100 kg to 1.46 at 200 kg. In conclusion, ASTM A36 steel is structurally adequate and can safely withstand the applied thermo-mechanical loads without premature fatigue failure. However, the reduced safety margins under elevated mechanical loads highlight the critical need for load control and targeted geometric reinforcements at structural joints to ensure long-term reliability. To ensure long-term reliability and operational safety in biomass gasification systems, it is imperative to implement targeted geometric reinforcements at connection points or substitute the standard carbon steel with high-temperature-resistant alloys.

Keywords:
Biomass gasification, char removal, fatigue life, finite element analysis, structural integrity

1. Introduction

Biomass gasification has emerged as a promising technology for converting renewable resources into clean and sustainable energy, particularly in addressing the growing demand for alternative energy sources and reducing dependence on fossil fuels (Prabir & Priyanka, 2024; Saputro et al., 2025; Supriatna et al., 2025). In this process, solid biomass is thermochemically converted into syngas at high temperatures, typically ranging from 800 °C to 1,200 °C (Lestari et al., 2025; Sadasivam et al., 2020; Supriatna et al., 2024). However, the efficiency and reliability of gasification systems are highly dependent on the performance of their mechanical components, especially those exposed to extreme thermal and mechanical conditions. One critical component in this system is the char removal unit, which plays a vital role in ensuring continuous operation by removing residual solid particles from the reactor.

Biomass gasification systems involve complex interactions between thermal, mechanical, and material factors that significantly influence structural performance. The mechanical properties of biomass-derived materials, such as char, are strongly affected by thermal conditions, where higher pyrolysis temperatures enhance hardness and stiffness due to structural evolution (Das et al., 2015). Temperature also plays a critical role during gasification, affecting particle characteristics, separation efficiency, and overall system performance (Yang et al., 2012), while variations in pyrolysis conditions modify char structure and porosity, influencing its interaction with mechanical components (Ates & Tezcan-Un, 2013). In practice, biomass gasification systems also face significant challenges related to tar and char by-products. Tar condensation can cause operational and environmental issues such as blockage, corrosion, and catalyst deactivation, making effective removal technologies essential (Zeng et al., 2020). Meanwhile, char accumulation can obstruct gas flow and reduce system efficiency, requiring mechanical char removal systems to ensure continuous operation. However, these systems operate under complex thermo-mechanical conditions, including high temperatures, cyclic loads, and continuous material flow, which can lead to structural degradation and fatigue failure (Yang et al., 2012).

The combined effects of thermal exposure and mechanical loading accelerate crack initiation and reduce material lifespan, with failures typically occurring at stress concentration points such as joints and welds. Furthermore, high-temperature operating environments can affect both particle removal efficiency and structural stability (Ates & Tezcan-Un, 2013), while dynamic effects such as vibration and damping significantly influence stress response and fatigue behavior, where inaccurate assumptions may lead to large errors in fatigue life prediction (Munson et al., 2017). Therefore, accurate prediction of fatigue behavior and crack propagation is essential to ensure structural reliability and effective maintenance planning (Alshoaibi & Ali-Fageehi, 2022).

To address these challenges, numerical simulation methods, particularly Finite Element Analysis (FEA), have become essential tools for evaluating structural integrity and fatigue performance. FEA enables detailed analysis of stress distribution, deformation, and crack propagation under complex thermo-mechanical loading conditions. Fracture mechanics approaches integrated with FEA, such as stress intensity factor evaluation and failure assessment diagrams, have been widely used to assess structural integrity and predict failure behavior in engineering components (Barrionuevo et al., 2020). Moreover, advanced simulations using ANSYS combined with fatigue models, such as Paris' law, allow accurate prediction of crack growth paths and fatigue life, with results showing strong agreement with experimental observations (Alshoaibi & Ali-Fageehi, 2022).

Despite extensive research on mechanical components in industrial systems, studies focusing specifically on char removal units in biomass gasification reactors remain limited. Most existing research emphasizes geometric optimization or material enhancement, while the combined influence of varying mechanical loads and high-temperature conditions on fatigue life has not been comprehensively investigated. Consequently, a detailed analysis that integrates structural behavior and fatigue performance under realistic thermo-mechanical operating conditions is still required.

To clearly position this study and highlight its novelty, a comparative analysis with several relevant previous studies is presented in Table 1. These selected studies represent major approaches commonly used in this field: fracture mechanics-based analysis, standard-based structural integrity assessment, and fatigue life prediction under mechanical loading.

Table 1. Comparative analysis with previous research.

Aspect	Our Study	Alshoaibi & Ali-Fageehi (2022)	Barrionuevo et al. (2020)	Fu et al. (2017)
Research Focus	Structural integrity and fatigue life of char removal system	Fatigue crack propagation and crack path prediction	Structural integrity using BS7910 and FAD	Fatigue life of screw blades under extreme load
Application	Biomass gasification system (real component)	Compact Tension Specimen (MCTS)	Penstock/pressure vessel	Screw sand washing machine
Methodology	ANSYS FEA (thermo-mechanical analysis)	ANSYS APDL + LEFM + Paris' Law	BS7910 + FEA + FAD	FEA + P-S-N curve + Soderberg method
Loading Condition	Combined thermal (800–1,200 °C) and mechanical load (100–200 kg)	Cyclic loading (mixed-mode I–II)	Internal pressure + cyclic loading	Extreme mechanical load
Thermal Effect	Explicitly considered	Not considered	Not dominant	Not considered
Key Parameters	Stress, strain, deformation, safety factor, fatigue life	Stress Intensity Factor, crack path, crack growth	Kr, Lr, fracture toughness	Stress, fatigue life, blade thickness
Failure Mechanism	Fatigue failure based on stress concentration	Crack initiation & propagation	Fracture and plastic collapse	Fatigue failure at blade root
Critical Findings	Load dominates fatigue life; temperature affects deformation	Geometry strongly affects crack trajectory	Structure safe if within FAD limit	Fatigue life increases with blade thickness
Limitation	No crack propagation modeling	Simplified geometry	Limited thermal consideration	No thermal effect

As observed in Table 1, previous studies generally focus on specific, isolated aspects of fatigue and structural analysis. For instance, Alshoaibi & Ali-Fageehi (2022) emphasize crack propagation behavior using fracture mechanics but limited their scope to simplified geometries. Barrionuevo et al. (2020) introduce a standards-based approach effective for evaluating structural safety under defect conditions, yet lacked consideration of thermo-mechanical coupling. Meanwhile, Fu et al. (2017) focus on fatigue life prediction of rotating components under extreme mechanical loads without incorporating temperature effects.

In contrast, the present study bridges these gaps by integrating combined thermo-mechanical loading conditions into the structural analysis of a real industrial component within a biomass gasification system. This approach allows for a more comprehensive evaluation of structural performance, considering not only mechanical stress but also the critical influence of high temperatures on material behavior. By bridging the gap between fracture mechanics, standards-based assessment, and practical engineering applications under realistic operating conditions, this study aims to provide a more holistic understanding of fatigue behavior in high-temperature systems.

Therefore, this study aims to evaluate the structural integrity and fatigue life of a char removal system in high-temperature gasification using ASTM A36 steel. The analysis is carried out under varying mechanical loads (100 kg, 150 kg, and 200 kg) and thermal conditions (800 °C, 1,000 °C, and 1,200 °C) using ANSYS-based Finite Element Analysis (FEA). Key parameters, including equivalent stress, elastic strain, total deformation, safety factor, and fatigue life, are systematically evaluated. The results are expected to provide a comprehensive understanding of the interaction between thermal and mechanical effects on structural reliability, as well as to offer design insights for improving the durability and operational safety of char removal systems in biomass gasification applications.

2. Methods and Materials

The research process begins with a literature study, followed by the design phase and the input of material properties. Subsequently, the researcher performs the meshing process and defines boundary conditions, which include force variables of 100 kg, 150 kg, and 200 kg, a fixed support, and thermal conditions at temperatures of 800 °C, 1,000 °C, and 1,200 °C. The simulation proceeds to the solution stage to obtain data on total deformation, equivalent stress, equivalent elastic strain, and safety factor. If the simulation run fails, the process reverts to the meshing stage; however, if successful, the researcher proceeds to data analysis and discussion until the study is completed. Figure 1 illustrates the gasification unit design, where the 3D design process is conducted using SolidWorks software. Subsequently, the simulation data collection for this research is performed using Ansys software. The detailed specifications of the equipment and materials are further elaborated in Table 2. The entirety of this research was conducted at the National Research and Innovation Agency (BRIN) and Universitas Pamulang.

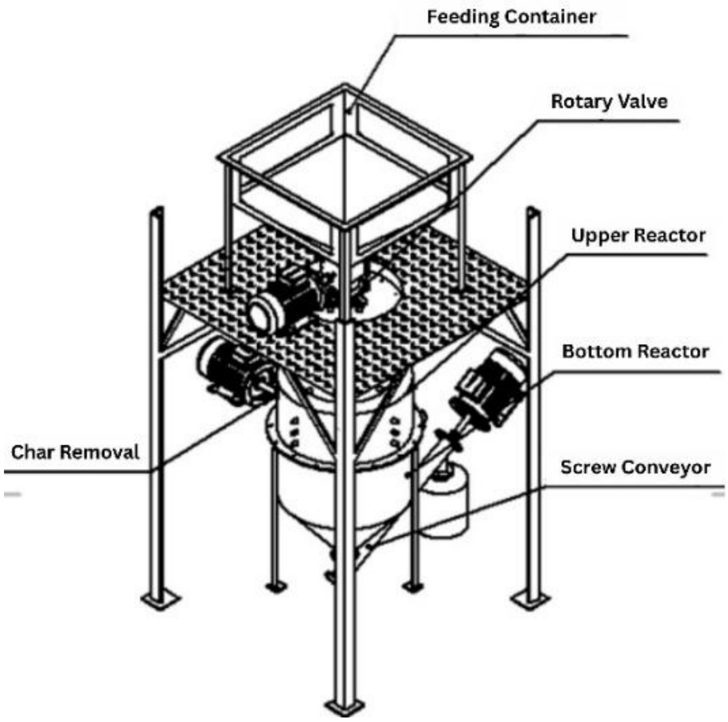

Figure 1. Gasification equipment design.

Table 2. Research tools and specifications.

Tool / Software	Specification / Description
SolidWorks 2022	Computer-Aided Design (CAD) software used for 3D modeling
ANSYS Workbench 2020 R1	Simulation software used for data acquisition and numerical analysis

2.1 Data Acquisition Techniques

The data acquisition process is conducted through four integrated stages to ensure the accuracy of the structural and thermal analysis. Initially, technical and dimensional data are collected by documenting engineering drawings and specifications of the gasification unit, specifically the char removal system. This phase includes the extraction of material properties, such as Young's modulus, yield strength, ultimate tensile strength, and density, from official technical datasheets and standards. Subsequently, operational load measurements are performed to determine the static and dynamic forces, alongside temperature monitoring using thermocouples to establish the thermal environment of the components. The numerical simulation phase is then executed using Ansys software, where specific boundary conditions including applied forces, rotational velocity, and torque are defined based on the previously gathered operational data. To ensure the reliability of the numerical results, a mesh sensitivity study is conducted prior to performing a comprehensive fatigue analysis to predict the structural life of the components under cyclic loading. As this study focuses on a purely computational and predictive approach, the reliability of the results is established through rigorous mesh sensitivity analysis to ensure numerical convergence. Empirical validation using a physical prototype under actual gasification conditions is acknowledged as a limitation of the current scope and is reserved for future investigations. All numerical results are systematically documented in the form of tables and graphical representations to facilitate a rigorous analysis and discussion.

2.2 Numerical Simulation Procedure Steps

The initial stage of this research involves geometric modeling, where the detailed design of the char removal unit is illustrated in Figure 2(a). The second step is the definition of material properties used in the simulation. In this study, ASTM A36 carbon steel is utilized, with its properties configured within the Ansys Engineering Data environment as shown in Figure 2(b). Specifically, the ASTM A36 material is defined with a density of 7,850 kg/m³. For the isotropic elasticity characteristics, a Young's Modulus of 200 GPa and a Poisson's Ratio of 0.26 are applied. Furthermore, the material strength parameters are established with a Tensile and Compressive Yield Strength of 250 MPa and a Tensile Ultimate Strength of 400 MPa. These parameters are essential to ensure the accuracy of the static structural results and the subsequent fatigue life analysis of the components.

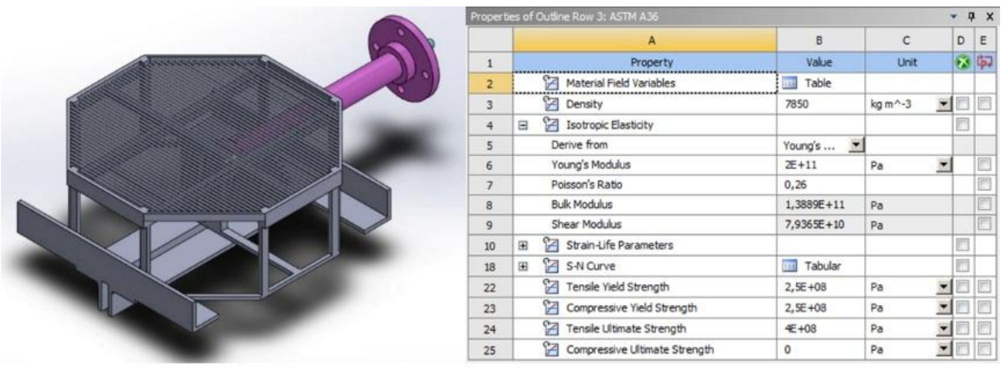

(a) (b)

Figure 2. Geometric model char removal (a) properties ASTM A36 in ANSYS (b).

It is important to note that for this specific comparative study, a simplified linear elastic model with constant baseline material properties was utilized across all temperature variations. Temperature-dependent property degradation was intentionally excluded to isolate and evaluate the direct impact of mechanical loading on structural fatigue.

The subsequent stage involves defining the Boundary Conditions, with the mechanical load being the primary parameter. As illustrated in Figure 3(a), the pressure is applied to the uppermost frame of the char removal unit, where the load is subsequently distributed throughout the entire structure. The input force values are 981 N, 1471 N, and 1962 N, which are derived from the gravitational force calculation:

$$F = m.g \tag{1}$$

Thermal Conditions are established to simulate the internal environment of the biomass gasification reactor. During operation, the reactor temperature can reach up to 1,200 °C; therefore, this study utilizes temperature variations of 800 °C, 1,000 °C, and 1,200 °C, as depicted in Figure 3(b). The final boundary condition is the Fixed Support, which defines the components that remain stationary. The selection of the fixed support corresponds to the geometry of the lower reactor section, specifically where the edges of the charcoal grate base interface with the bottom part of the reactor, as shown in Figure 3(c).

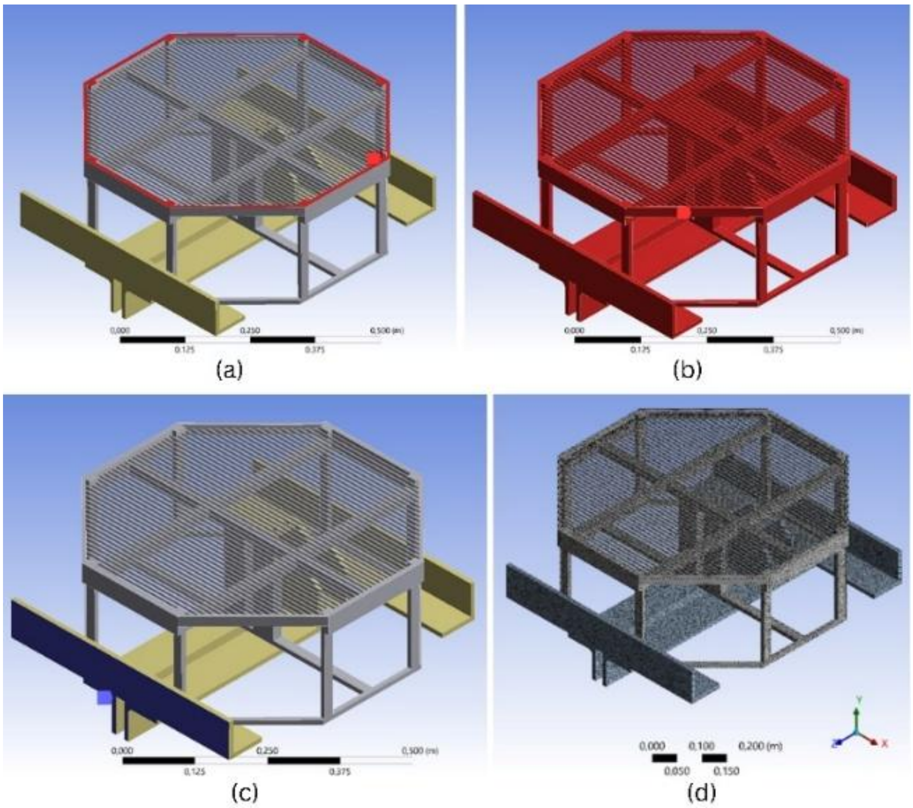

Figure 3. Mechanical load (a), thermal condition (b), fixed support (c), and meshing (d).

Meshing is employed to discretize the model into small elements, ensuring that the numerical calculations achieve high accuracy. To ensure grid independence, a mesh sensitivity study was conducted by systematically evaluating element sizes of 0.005 m, 0.003 m, and 0.002 m. While the 0.005 m configuration computed quickly, further refinement was necessary to accurately capture stress concentrations at the structural joints. The refinement to a 0.003 m element size yielded stable and converged results. An attempt to refine the mesh further to 0.002 m was executed; however, this exceeded the physical memory capacity (8 GB RAM) of the computational hardware, resulting in a solver crash. As illustrated in Figure 3(d), the mesh is distributed densely and uniformly across the entire surface of the char removal unit. This refined distribution indicates a high level of analytical detail in the simulation, resulting in a total of 832,003 nodes and 469,683 elements. In this context, nodes represent the grid intersection points, while elements are the fundamental structural subdivisions computed during the simulation. The substantial number of elements and nodes signifies that the simulation requires significant computational resources; however, it provides more accurate analytical results for parameters such as stress, strain, and fatigue-induced damage. By implementing an ideal mesh density, this simulation is expected to yield valid and representative calculations that closely align with actual operational conditions.

To ensure a robust numerical analysis, the initial and boundary conditions of the simulation were explicitly defined. The simulation was initiated by establishing the initial conditions, which include the geometry, material properties, and mesh configuration of the char removal system. The geometry was created using SolidWorks and subsequently imported into ANSYS Workbench 2020 R1. ASTM A36 steel was selected as the structural material, defined with a Young's Modulus of 200 GPa, a Poisson's Ratio of 0.26, a yield strength of 250 MPa, an ultimate tensile strength of 400 MPa, and a density of 7,850 kg/m³. The meshing process employed a fine mesh configuration, generating 832,003 nodes and 469,683 elements to ensure high computational accuracy. Furthermore, the boundary conditions were defined to accurately represent the actual operating environment of the biomass gasification system. Mechanical loads of 100 kg, 150 kg, and 200 kg, equivalent to vertical forces of 981 N, 1471 N, and 1,962 N, respectively, were applied to the upper frame of the char removal unit. Additionally, thermal conditions of 800 °C, 1,000 °C, and 1,200 °C were applied to simulate the internal operating temperatures of the gasification reactor. Finally, a fixed support was implemented at the lower reactor frame to constrain structural displacement, mirroring the actual mounting conditions during operation. To provide a clear overview of the overall simulation setup, the detailed baseline conditions and parameters applied in this study are summarized in Table 3.

Table 3. Summary of simulation baseline conditions.

Parameter	Value / Condition	Description
Material	ASTM A36 Steel	Structural material used for char removal unit
Young's Modulus	200 GPa	Elastic modulus of ASTM A36
Poisson's Ratio	0.26	Poisson's ratio of the material
Yield Strength	250 MPa	Yield limit of material
Ultimate Tensile Strength	400 MPa	Maximum tensile strength
Density	7,850 kg/m³	Material density
Mechanical Load	100 kg, 150 kg, 200 kg	Applied vertical load on upper frame
Equivalent Force	981 N, 1,471 N, 1,962 N	Force converted from mass
Thermal Condition	800 °C, 1,000 °C, 1,200 °C	Reactor operating temperature
Boundary Condition	Fixed Support	Applied at lower reactor frame
Software	ANSYS Workbench 2020 R1	Simulation software
Mesh Type	Fine mesh	Mesh density applied to the geometry
Number of Nodes	832,003	Total simulation nodes
Number of Elements	469,683	Total simulation elements
Analysis Type	Static Structural & Fatigue Analysis	Simulation approach used

3. Results and Discussions

3.1 Thermo-Mechanical Structural Response under Variable Loads

The structural behavior of the char removal unit is governed by the combined effects of mechanical loading and temperature-dependent material degradation. Across all evaluated conditions, the results demonstrate that mechanical load predominantly controls the magnitude of stress, strain, and deformation, whereas temperature primarily affects their spatial distribution. This trend is consistently observed in the simulation results presented in Figures 4–8.

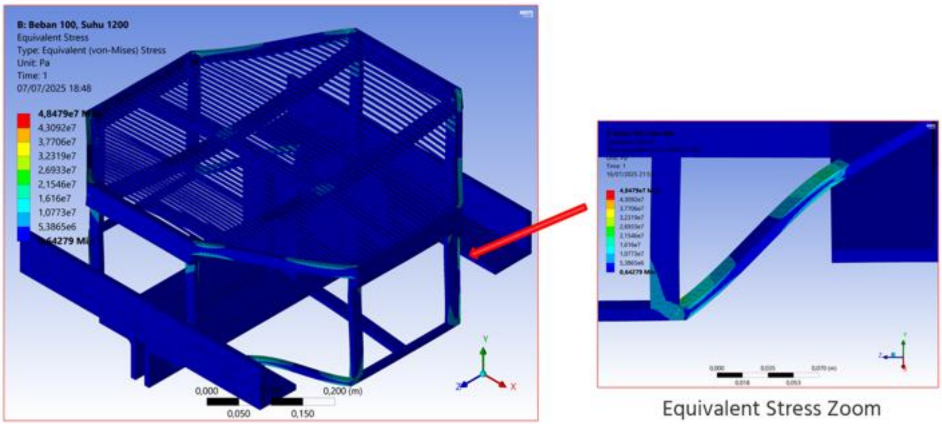

Figure 4. Full structural view and identification of the critical stress concentration region at the structural joints.

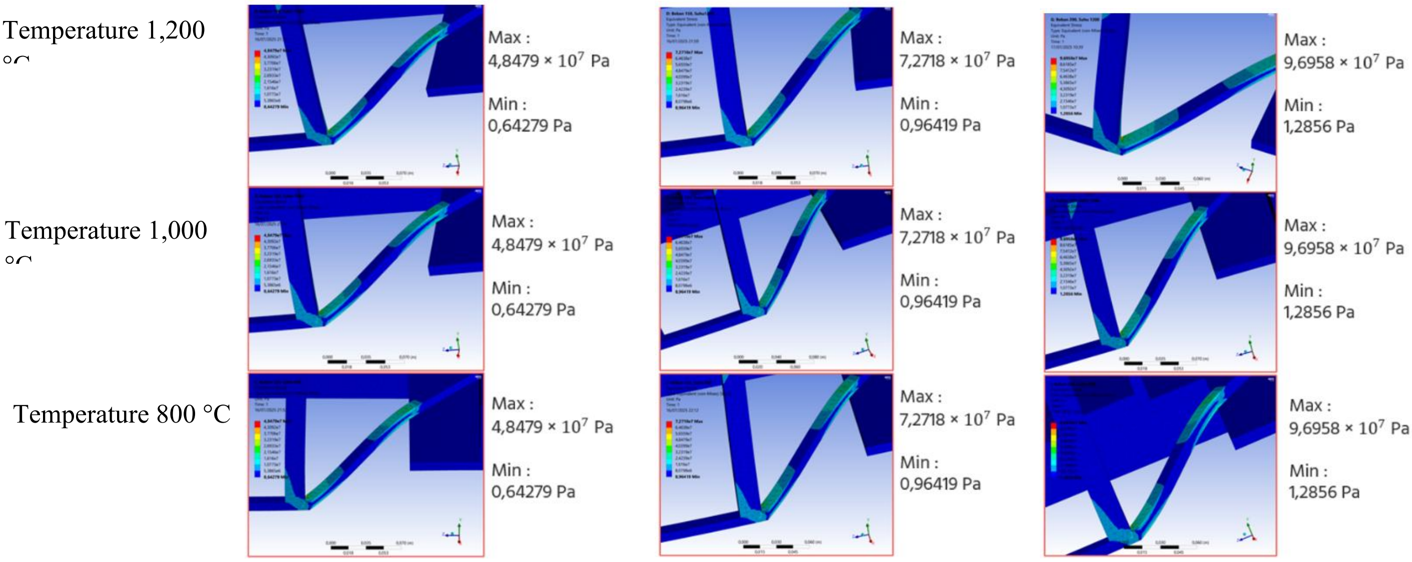

Figure 5. Detailed comparison of equivalent stress distribution at the critical joint under varying mechanical loads (100 kg, 150 kg, 200 kg) and thermal conditions (800 °C, 1,000 °C, 1,200 °C).

To clearly illustrate the structural response and address the subtle changes induced by thermal variations, Figure 4 identifies the critical stress concentration region, which is consistently located at the structural joints of the char removal unit. A detailed, zoomed-in observation of this critical region under varying loads and temperatures is presented in Figure 5. As shown in the localized stress contours, the peak equivalent stress is predominantly driven by the mechanical load. However, adjusting the visualization focus clearly reveals that temperature variations (800 °C, 1,000 °C, and 1,200 °C) visibly affect the spatial distribution and expansion of the high-stress zones. Higher temperatures cause the high-stress contours to spread wider across the joint due to localized material softening and a reduction in stiffness.

For the baseline condition of 100 kg, the maximum equivalent stress remains constant at 48.479 MPa across temperatures of 800 °C, 1,000 °C, and 1,200 °C, confirming that temperature does not significantly influence peak stress values. A similar pattern is observed in elastic strain and total deformation (illustrated in Figure 6), where identical peak values are maintained, but the affected zones become broader at elevated temperatures. This behavior reflects how thermal variations influence the spatial expansion and redistribution of the high-strain zones across the joint geometry, even when the underlying macroscopic material stiffness parameters are held constant in the numerical setup.

.

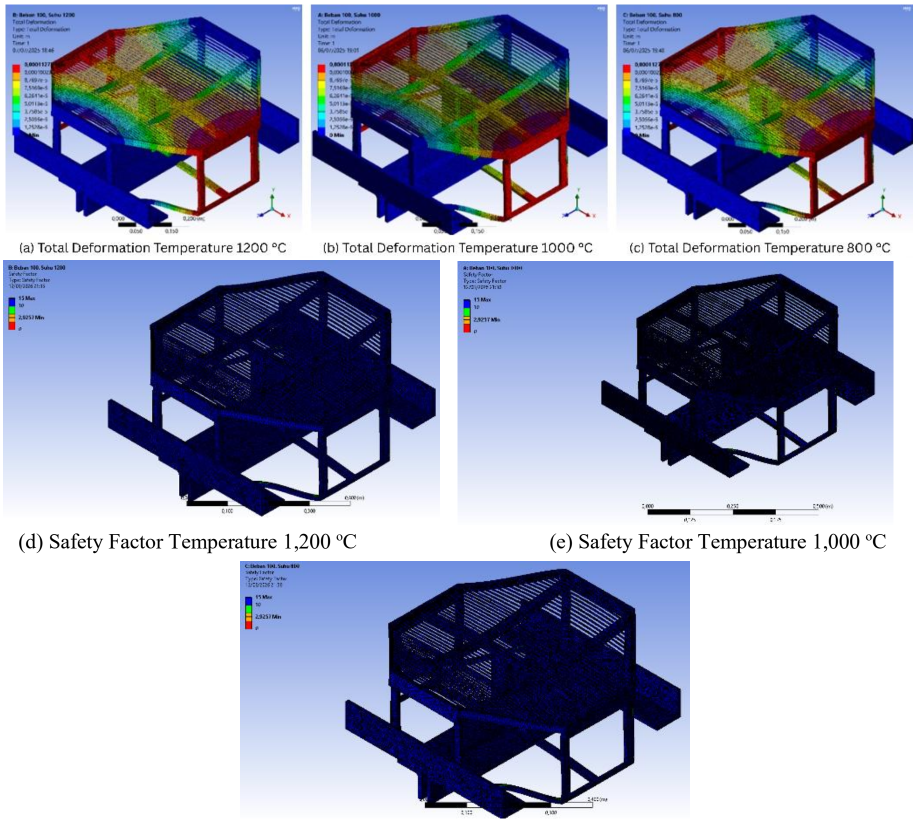

(a) Total Deformation Temperature 1200 °C (b) Total Deformation Temperature 1000 °C (c) Total Deformation Temperature 800 °C

(d) Safety Factor Temperature 1,200 °C (e) Safety Factor Temperature 1,000 °C

(f) Safety Factor Temperature 800 °C

Figure 6. Total deformation temperature 1,200 °C (a), total deformation temperature 1,000 °C (b), total deformation temperature 800 °C (c), safety factor temperature 1,200 °C (d), safety factor temperature 1,000 °C (e), safety factor temperature 800 °C (f) for the baseline condition of 100 kg.

When the load increases to 150 kg, as shown in Figure 7, the structural response intensifies significantly. The maximum equivalent stress rises to 72.718 MPa, accompanied by an increase in elastic strain (3.9948×10^{-4} m/m) and total deformation (1.6913×10^{-4} m). Despite these increases, the effect of temperature remains consistent with the previous case, influencing only the spread of deformation rather than its magnitude. Notably, the minimum fatigue safety factor decreases to 1.95. Despite this reduction, the value remains comfortably above unity, indicating that the structure operates within safe margins and successfully maintains an infinite design life of 1×10^6 cycles under this specific load.

At the maximum load of 200 kg, the structural response reaches a critical level, as presented in Figure 8. The maximum equivalent stress increases to 96.958 MPa, while the elastic strain and total deformation increase to 5.3264×10^{-4} m/m and 2.2551×10^{-4} m, respectively. These results confirm a near-linear scaling of mechanical response with applied load. At the maximum load of 200 kg, the minimum fatigue safety factor drops further to 1.46. Although this value indicates a reduced safety margin compared to the baseline, it remains strictly above unity. This ensures the structure does not transition into a failure-dominated regime and continues to successfully sustain 1×10^6 cycles without immediate risk of crack initiation at the structural joints.

A direct comparison across the three loading conditions reveals a clear load-dependent scaling of the structural response. The maximum equivalent stress increases from 48.479MPa at 100 kg to 72.718 MPa at 150 kg, and further to 96.958 MPa at 200 kg, indicating a near-linear relationship between applied load and stress intensity. A similar trend is observed in the elastic strain, which rises from 2.6632×10^{-4} m/m to 3.9948×10^{-4} m/m and reaches 5.3264×10^{-4} m/m at the highest load. Likewise, total deformation increases proportionally from 1.1275×10^{-4} m to 1.6913×10^{-4} m and finally 2.2551×10^{-4} m.

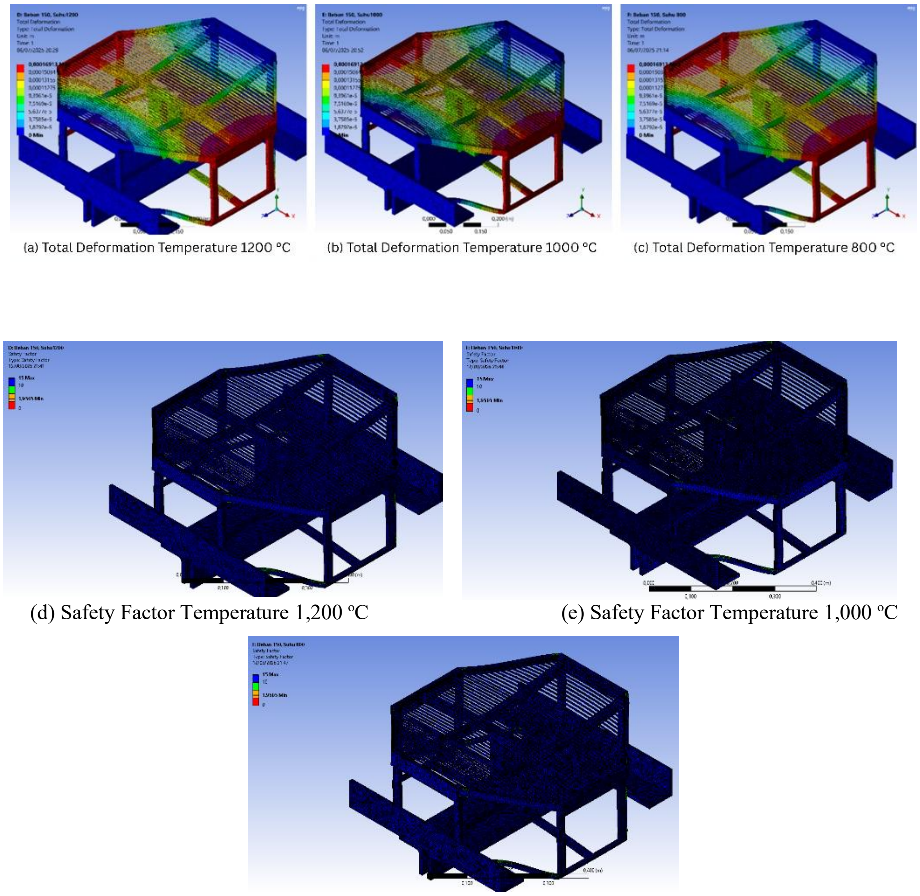

(a) Total Deformation Temperature 1200 °C (b) Total Deformation Temperature 1000 °C (c) Total Deformation Temperature 800 °C

(d) Safety Factor Temperature 1,200 ºC (e) Safety Factor Temperature 1,000 ºC

(f) Safety Factor Temperature 800 ºC

Figure 7. Total deformation temperature 1,200 °C (a), total deformation temperature 1,000 °C (b), total deformation temperature 800 °C (c), safety factor temperature 1,200 °C (d), safety factor temperature 1,000 °C (e), safety factor temperature 800 °C (f) for the 150 kg.

This consistent increase across all mechanical parameters confirms that the structural response is primarily governed by the magnitude of the applied load, following elastic scaling behavior. In contrast, temperature variations do not significantly affect the peak values of stress, strain, or deformation, but instead contribute to the spatial expansion of the affected regions. This indicates that within the investigated range, temperature acts as a secondary factor, amplifying deformation distribution rather than increasing structural intensity.

More importantly, while the maximum stress increases linearly, the structural reliability, evaluated through the minimum fatigue safety factor, decreases proportionally. The fatigue safety factor drops from 2.92 at 100 kg to 1.95 at 150 kg, and down to 1.46 at 200 kg. However, because all safety factors remain > 1, the fatigue life across all three scenarios consistently achieves the infinite life threshold of 1×10^6 cycles. This confirms that within the evaluated 100–200 kg load range, the char removal unit remains structurally safe from high-cycle fatigue failure, though the safety margin is substantially narrowed at peak loads. To clearly present these quantitative changes for thorough analysis, the extracted values of stress, strain, deformation, and safety factor under all evaluated thermo-mechanical conditions are summarized in Table 4.

To quantitatively evaluate the structural degradation, a percentage-based analysis of the data presented in Table 4 reveals a direct proportional relationship in the static mechanical response. A 50% increase in the applied mechanical load (from 100 kg to 150 kg) results in an exact 50.0% increase in the maximum equivalent stress (from 48.479 MPa to 72.718 MPa). Similarly, doubling the load to 200 kg (a 100% increase) proportionally doubles the maximum stress to 96.958 MPa. However, interpreting these linear static results alongside the dynamic fatigue data demonstrates a severe, non-linear degradation. While the stress scales linearly, interpreting these static results alongside the dynamic fatigue data demonstrates a proportional reduction in safety margins. The initial 50% increase in load results in a 33% reduction in the fatigue safety factor (from 2.92 to 1.95). Doubling the initial load to 200 kg halves the safety factor (a 50% reduction, down to 1.46). Despite this structural degradation, the component maintains a fatigue cycle life of 1×10^6, verifying that the unit operates safely within its high-cycle fatigue limits without entering a critical failure regime.

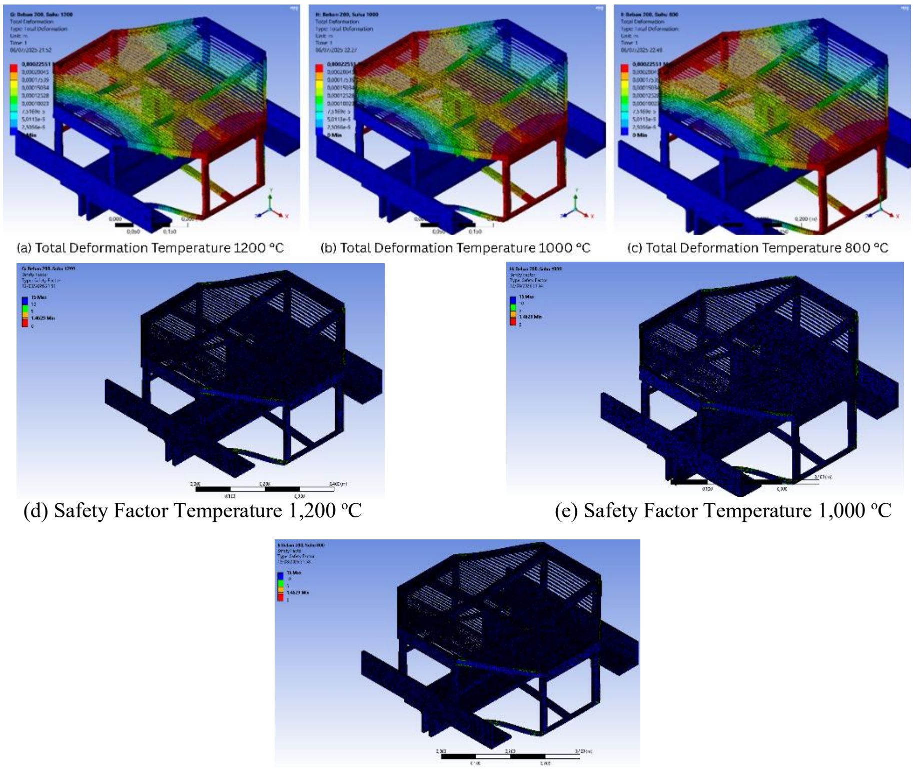

(a) Total Deformation Temperature 1200 °C (b) Total Deformation Temperature 1000 °C (c) Total Deformation Temperature 800 °C

(d) Safety Factor Temperature 1,200 °C (e) Safety Factor Temperature 1,000 °C

(f) Safety Factor Temperature 800 °C

Figure 8. Total deformation temperature 1,200 °C (a), total deformation temperature 1,000 °C (b), total deformation temperature 800 °C (c), safety factor temperature 1,200 °C (d), safety factor temperature 1,000 °C (e), safety factor temperature 800 °C (f) for the 200 kg.

The observed structural behavior can be explained through the interaction between load-driven elastic response and temperature-induced material degradation. The increase in mechanical load directly amplifies the internal stress and strain following a near-linear elastic scaling, as evidenced by the proportional rise in stress, strain, and deformation from 100 kg to 200 kg. However, this mechanical response is further influenced by thermal effects, particularly through the degradation of Young's modulus at elevated temperatures. As temperature increases, the reduction in atomic bonding stiffness facilitates wider deformation propagation, resulting in an expansion of strain distribution rather than an increase in peak stress values.

In addition, stress concentration plays a critical role in governing structural failure. The simulation results consistently indicate that critical regions are localized at frame intersections and joint connections, where geometric discontinuities act as stress risers. Under cyclic loading conditions, these regions become the primary sites for crack initiation. This behavior is further intensified by thermo-mechanical coupling, where repeated loading combined with elevated temperatures accelerates material degradation. Consequently, thermo-mechanical fatigue (TMF) emerges as the dominant failure mechanism, surpassing the influence of static strength criteria such as safety factor alone. This explains why structures with comparable safety factor values can exhibit drastically different fatigue lives under varying load conditions.

Table 4. Summary of extreme values for structural responses under varying thermo-mechanical conditions.

Parameter	Load	800 °C	1,000 °C	1,200 °C
Max. Equivalent Stress (MPa)	100 kg	48.479	48.479	48.479
	150 kg	72.718	72.718	72.718
	200 kg	96.958	96.958	96.958
Max. Elastic Strain (× 10^{-4} m/m)	100 kg	2.663	2.663	2.663
	150 kg	3.994	3.994	3.994
	200 kg	5.326	5.326	5.326
Max. Total Deformation (× 10^{-4} m)	100 kg	1.127	1.127	1.127
	150 kg	1.691	1.691	1.691
	200 kg	2.255	2.255	2.255
Min. Safety Factor	100 kg	2.920	2.920	2.920
	150 kg	1.950	1.950	1.950
	200 kg	1.460	1.460	1.460

The results of this study are consistent with previous findings indicating that thermal gradients predominantly influence the distribution and expansion of stress–strain regions rather than significantly increasing the peak equivalent stress (Bhowmik et al., 2020; Nwigbo & Nwoye, 2015). This behavior is governed by non-uniform thermal expansion, which generates internal constraints and redistributes stress fields across the structure. As temperature increases, the reduction in elastic modulus and yield strength of low-carbon steels such as ASTM A36 leads to a progressive enlargement of high-strain zones, even when the applied mechanical load remains constant (Agrawal et al., 2025; Nikulin et al., 2021). In contrast, studies on high-temperature alloys reveal significantly improved structural stability due to their superior resistance to thermal softening and creep deformation (Cao et al., 2021). Materials containing chromium and nickel are capable of maintaining higher safety factors under extreme temperatures, highlighting the critical role of material selection in thermo-mechanical applications.

Moreover, geometric optimization has been shown to substantially influence fatigue performance by reducing stress concentration and improving load distribution (Sun et al., 2024; Zhu et al., 2018) . However, the present study indicates that fatigue life in the char removal unit is more sensitive to cyclic load variation than to temperature alone, suggesting that thermo-mechanical fatigue (TMF) behavior governs long-term failure. This interaction between cyclic loading and temperature has been widely recognized as a key factor in structural degradation under high-temperature service conditions, where both material properties and design configuration must be optimized simultaneously to achieve reliable performance. Furthermore, while (Fu et al., 2017) achieved an operational life of 35 years by optimizing blade thickness, this research shows that for the char removal unit, the fatigue life is more sensitive to operational load variations than to temperature alone. This suggests that while ASTM A36 is economically viable, it may require localized geometric reinforcement or high-temperature coating to match the industrial reliability standards established in previous literature.

3.2 Fatigue Life Analysis

The fatigue analysis results, as illustrated in Figure 9, demonstrate the robust endurance of the char removal unit under the specified operating conditions. Across all applied mechanical loads (100 kg, 150 kg, and 200 kg), the structure consistently achieves a fatigue life of 1×10^6 cycles. In the context of the ANSYS Stress-Life approach utilizing the Goodman mean stress theory, a life of 10^6 cycles denotes an 'infinite life' design threshold for steel components. This behavior indicates that the operational stresses generated by the 100–200 kg loads remain comfortably below the endurance limit of the ASTM A36 material.

Although the total cycle life remains constant at the infinite threshold, the decreasing trend in the fatigue safety factor (from 2.92 to 1.46) signifies that the margin against fatigue failure is actively narrowing as the load increases. The structural joints and frame intersections continue to act as stress risers; however, the stress concentration at these regions is not severe enough to initiate low-cycle fatigue (LCF) or rapid crack propagation under the evaluated load limits.

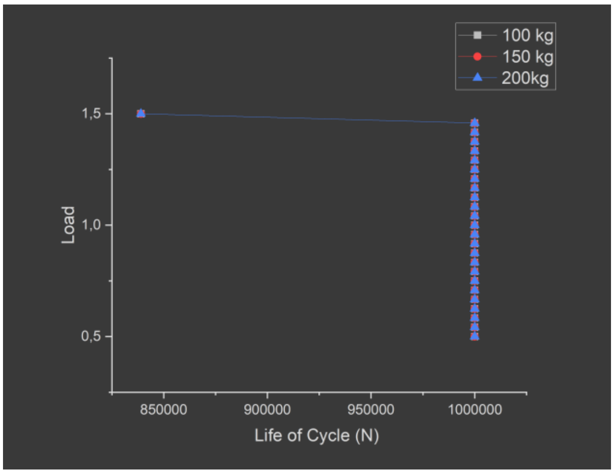

Figure 9. Fatigue life curves of the char removal unit under varying mechanical loads (100 kg, 150 kg, and 200 kg).

Therefore, as long as the operational mass does not significantly exceed 200 kg, the char removal unit is predicted to operate reliably without premature fatigue failure. Maintaining these operational thresholds and ensuring high-quality fabrication (such as proper welding techniques) at the critical joints are sufficient to guarantee the long-term serviceability of the biomass gasification component (Al-Mukhtar & Koenke, 2025; Alshoaibi et al., 2021; Beber & Schneider, 2020).

4. Conclusions

This study successfully evaluates the structural integrity and fatigue performance of a char removal system operating under high-temperature gasification conditions using ANSYS-based Finite Element Analysis. Based on the quantitative data extracted from the simulations, it is concluded that mechanical load acts as the primary driver of structural degradation, dictating the peak magnitude of the structural response. The maximum equivalent stress scales linearly from 48.479 MPa at a 100 kg load to 96.958 MPa at a 200 kg load. Conversely, temperature variations (800 °C to 1,200 °C) do not significantly alter the peak stress values but crucially expand the spatial distribution of strain and deformation due to the thermal softening of the material.

Furthermore, as demonstrated by the fatigue life curve, this load-driven stress amplification leads to a non-linear, rapid degradation of the component's operational life. Increasing the applied load from 100 kg to 200 kg reduces the fatigue safety margin, with the minimum safety factor dropping from 2.92 to 1.46. Despite this reduction, the values remain strictly above unity, allowing the structure to consistently maintain an infinite fatigue life of 1×10^6 cycles across all tested scenarios. The stress concentrations are localized at structural joints, but they remain below the critical threshold for crack initiation.

These data-driven findings definitively indicate that standard ASTM A36 steel is structurally adequate and highly reliable for the char removal unit within the 100–200 kg load range. While the component is not currently vulnerable to premature fatigue failure, the halved safety margin at the maximum load suggests that any unexpected dynamic overloading could risk crack initiation. Finally, while this computational study provides critical design insights, future research will focus on the empirical validation of these numerical findings through physical testing of the char removal unit prototype under actual operational gasification conditions.

Acknowledgments

This research was supported financially by Joint Research Collaboration Funding within the Energy and Manufacturing Research Organization of the National Research and Innovation Agency (BRIN) No. 6/III.3/HK/2026. This research is a part of the "Energy Conversion for Gasification Products" Research Group activity at the Research Centre for Energy Conversion Technology, National Research and Innovation Agency.

References

Agrawal, A. P., Ali, S., Kumar, V., & Gupta, P. (2025). Investigating the impact of heat treatment on mechanical behaviour of A36 low-carbon steel. *Archives of Thermodynamics*, 141–149. https://doi.org/10.24425/ather.2025.156586

Al-Mukhtar, A., & Koenke, C. (2025). Fatigue life analysis of cruciform specimens under biaxial loading using the Paris equation. *Metals*, *15*(6), 579. https://doi.org/10.3390/met15060579

Alshoaibi, A. M., & Ali-Fageehi, Y. (2022). 3D modelling of fatigue crack growth and life predictions using ANSYS. *Ain Shams Engineering Journal*, *13*(4), 101636. https://doi.org/10.1016/j.asej.2021.11.005

Alshoaibi, A. M., Ghazwani, M. A., & Hakami, M. H. (2021). Fatigue life and reliability assessment of metal structures. *Engineering Solid Mechanics*, *9*, 13–22. https://doi.org/10.5267/j.esm.2020.7.001

Ates, F., & Tezcan-Un, U. (2013). Production of char from hornbeam sawdust and its performance evaluation in the dye removal. *Journal of Analytical and Applied Pyrolysis*, *103*, 159–166. https://doi.org/10.1016/j.jaap.2013.01.021

Barrionuevo, G. O., Guerrero, B. A., & Walczak, M. (2020). Computational fracture mechanics: evaluation of the structural integrity in a penstock applying the BS7910 standard and finite element analysis. *IOP Conference Series: Materials Science and Engineering*, *925*(1). https://doi.org/10.1088/1757-899X/925/1/012023

Beber, V. C., & Schneider, B. (2020). Fatigue of structural adhesives under stress concentrations: Notch effect on fatigue strength, crack initiation and damage evolution. *International Journal of Fatigue*, *140*, 105824. https://doi.org/10.1016/j.ijfatigue.2020.105824

Bhowmik, M., Banerjee, P., & Bhowmik, M. K. (2020). A theoretical study of thermal stress for engineering applications. In *Applications and techniques for experimental stress analysis* (pp. 176–201). IGI Global https://doi.org/10.4018/978-1-7998-1690-4.ch012

Cao, B., Zhao, Y., Yang, T., & Liu, C. T. (2021). $L1_2$-strengthened Co-rich alloys for high-temperature structural applications: a critical review. *Advanced Engineering Materials*, *23*(10). https://doi.org/10.1002/adem.202100453

Das, O., Sarmah, A. K., & Bhattacharyya, D. (2015). Structure-mechanics property relationship of waste derived biochars. *Science of the Total Environment*, *538*, 611–620. https://doi.org/10.1016/j.scitotenv.2015.08.073

Fu, Y.-F., Gong, J., Li, P.-W., & Yang, Z.-M. (2017). Fatigue life assessment of screw blades in screw sand washing machine under extreme load. *American Journal of Mechanical Engineering*, *5*(1), 1–7. https://doi.org/10.12691/ajme-5-1-1

Lestari, P., Surjosatyo, A., Dafiqurrohman, H., Saputro, B. A., Dhani, S. T., & Nami, H. (2025). Optimization of syngas production and biochar utilization from municipal solid waste (MSW) via integrated pyrolysis-gasification for electricity generation. *Bioresource Technology Reports*, *31*, 102217. https://doi.org/10.1016/j.biteb.2025.102217

Munson, K., Kihm, F., & Halfpenny, A. (2017). Improving the accuracy of dynamic vibration fatigue simulation. *SAE International Journal of Engines*, *10*(2), 2017-01–0333. https://doi.org/10.4271/2017-01-0333

Nikulin, S. A., Rogachev, S. O., Nikolaev, Y. A., Vasiliev, S. G., Belov, V. A., & Turilina, V. Y. (2021). High-temperature mechanical properties of low-carbon steel used for the manufacture of core catcher vessel. *Progress in Nuclear Energy*, *142*, 104015. https://doi.org/10.1016/j.pnucene.2021.104015

Nwigbo, S. C., & Nwoye, C. F. (2015). Thermal and residual stress analysis on A36 steel plate brazed with a known volume of Zn50 brazing alloy (filler metal). *Journal of Failure Analysis and Prevention*, *15*(6), 924–931. https://doi.org/10.1007/s11668-015-0037-2

Sadasivam, S., Zagorščak, R., Thomas, H. R., Kapusta, K., & Stańczyk, K. (2020). Experimental study of methane-oriented gasification of semi-anthracite and bituminous coals using oxygen and steam in the context of underground coal gasification (UCG): Effects of pressure, temperature, gasification reactant supply rates and coal rank. *Fuel*, *268*, 117330. https://doi.org/10.1016/j.fuel.2020.117330

Saputro, B. A., Surjosatyo, A., Sari, W. R., Dafiqurrohman, H., Qossam, I. Al, & Lestari, P. (2025). Hydrogen-rich syngas production of solid waste supercritical water gasification multi-objective process optimization. *International Journal of Renewable Energy Development*, *14*(4), 629–645. https://doi.org/10.61435/ijred.2025.60848

Sun, Y., Song, D., Sun, S., & Liu, Y. (2024). Study on fatigue performance and topology optimization of cast steel bifurcation joint under alternating load. *Engineering Research Express*, *6*(4), 045107. https://doi.org/10.1088/2631-8695/ad84a1

Supriatna, N. K., Zuldian, P., Aminuddin, Purawiardi, I., Aprianti, N., Gunawan, Y., Fariza, O., Raksodewanto, A. A., Alamsyah, R., Hasanuzzaman, M., & Surjosatyo, A. (2024). Experimental investigation and performance evaluation of Samanea saman leaves and twigs gasification from urban residential garden waste as alternative future energy. *Bioresource Technology Reports*, *27*, 101950. https://doi.org/10.1016/j.biteb.2024.101950

Supriatna, N. K., Zuldian, P., Gunawan, Y., Aprianti, N., Aminuddin, Nurjanah, N., Umi Culsum, N. T., Purawiardi, R. I., Prasetya, A., Tjahjono, E. W., Alamsyah, R., & Surjosatyo, A. (2025). Kinetic and thermodynamic analysis of garden waste gasification for clean syngas production. *Thermal Science and Engineering Progress*, *68*, 104239. https://doi.org/https://doi.org/10.1016/j.tsep.2025.104239

Yang, S. I., Chung, I. L., & Wu, S. R. (2012). An experimental study of the influence of temperature on char separation in a moving granular bed. *Powder Technology*, *228*, 121–127. https://doi.org/10.1016/j.powtec.2012.05.006

Zeng, X., Ueki, Y., Yoshiie, R., Naruse, I., Wang, F., Han, Z., & Xu, G. (2020). Recent progress in tar removal by char and the applications: A comprehensive analysis. *Carbon Resources Conversion*, *3*, 1–18. https://doi.org/10.1016/j.crcon.2019.12.001

Zhu, B. J., Wang, T., & Zhang, L. X. (2018). Mechanical Behavior of Assembled Steel Dampers with Optimized Shapes. *Key Engineering Materials*, *763*, 959–966. https://doi.org/10.4028/www.scientific.net/KEM.763.959